

# Variation in bulk density of granitic rock samples at mild temperature range

Lekan Olatayo Afolagboye <sup>a, \*</sup>, Adenike Helen Adedeji <sup>a</sup>, Olubunmi Oluwadare Owoyemi <sup>b</sup> and Yusuf Ademola Abdu-Raheem <sup>a</sup>

<sup>a</sup> Department of Geology, Ekiti State University, Ado-Ekiti, Nigeria.

<sup>a</sup> Department of Geology, Kwara State University, Malete, Nigeria.

## Article History:

Received: 02 February 2024.

Revised: 24 May 2025.

Accepted: 17 September 2025.

## ABSTRACT

Numerous laboratory investigations have explored the properties of various rocks subjected to high temperatures rarely encountered in rock engineering applications. This study investigates the variation in bulk density of fine-grained granite (FGG) under mild temperatures (20°C–200°C), relevant to rock engineering applications such as geothermal systems and radioactive waste storage. The objectives are to quantify changes in mass, volume, and bulk density of FGG samples and identify underlying mechanisms through microscopic analysis. Cylindrical core samples (50 mm diameter × 100 mm height) were extracted from a granite outcrop in Ado-Ekiti, southwestern Nigeria, with a core drilling machine, following ISRM standards. Mass and volume were measured before, during, and after heating at 20°C intervals up to 200°C in an electric oven. Bulk density was calculated using ISRM standards based on the measured mass and volume at selected mild temperature intervals. Results show a decrease in mass and an increase in volume with rising temperature, leading to a reduction in bulk density. The average percentage of mass loss, volume increase, and bulk density decrease was higher during heating than after cooling. In addition, microscopic analysis indicated a progressive increase in microcrack density, with distinct trans-granular cracks forming across feldspar grains at 200 °C. The findings reveal the potential impact of mild thermal exposure on granite's structural integrity, which is relevant for rock engineering applications in environments subject to moderate thermal fluctuations.

**Keywords:** Bulk density, Granite, Mass loss, Mild temperature range.

## 1. Introduction

Unlike rock outcrops, rocks beneath the Earth's surface are exposed to higher temperatures due to the geothermal gradient—a progressive increase in temperature with depth, typically ranging from 20° to 30 °C per kilometer. Moreover, several rock engineering applications such as the disposal of radioactive waste [1], subsurface coal gasification [2], tunnel restoration after a fire, and in situ combustion enhanced oil recovery [3], expose buried or subsurface rocks to elevated temperatures. Recent studies have focused on the behaviour of rocks at high temperatures due to their relevance in rock engineering applications. Elevated temperatures significantly affect rock properties and behaviour, but the impact varies with rock type, structure, and temperature gradients [4, 5]. Understanding these effects is essential for predicting rock performance in subsurface environments and engineering designs.

Research indicates that rock properties such as volume, permeability, and porosity tend to increase with rising temperatures [1, 6–8]. In contrast, bulk density (BD), compressive and tensile strength, fracture roughness, and thermal conductivity generally decrease under thermal influence [9–12]. These variations are commonly attributed to thermal or structural damage, including the propagation of existing microcracks and the initiation of new ones, driven by differences in thermal expansion among mineral crystals and crystallographic axes [13–15]. Additionally, irreversible chemical reactions—such as clay mineral

decomposition and calcite transformation—also contribute to these changes [16, 17].

Most studies suggest that significant thermal damage in rocks occurs at temperatures above 300°C–400°C [10, 18–20]. However, current rock engineering applications rarely expose host rocks to temperatures exceeding 300°C [19, 21]. In practice, subsurface rocks reaching temperatures above 400 °C are found only at depths of around 17 km—far below the typical depth of engineering operations. According to [22], the temperature of rocks at the Mponeng gold mine in South Africa, located approximately 4000 m deep, is 66 °C. The temperature of most geothermal systems is about 200 °C and can be as low as 80 °C [23]. In radioactive waste storage, canister surface temperatures are limited to 100 °C [24], and even after years of radioactivity, the temperature of surrounding host rocks at depths of 1000 m rarely exceeds 165 °C [25]. Therefore, the effects of temperatures below 200 °C on rock properties warrant greater attention, as they are more relevant to practical applications.

Bulk density (BD) is a fundamental physical property of rocks and plays a crucial role in engineering calculations and design. Previous studies have shown that BD decreases with increasing temperature, although the rate of change varies among rock types due to differences in mineral composition [12, 26]. Most research, however, has focused on broad temperature ranges (up to 1200 °C) with wide testing intervals [6,

\* Corresponding author. E-mail address: [lekan.afolagboye@eksu.edu.ng](mailto:lekan.afolagboye@eksu.edu.ng) (L. O. Afolagboye).

10, 12, 27–29]. Such extreme conditions do not realistically represent the moderate thermal environments encountered in practical rock engineering applications. Moreover, studies that investigate temperature increments relevant to these conditions—particularly within the mild temperature range (MTR) of 20 °C to 200 °C—remain relatively scarce. For instance, [27] employed a 100 °C testing interval, while [6, 10, 12] adopted intervals of 200 °C. [29] used 50 °C intervals up to 200 °C and then switched to 100 °C intervals thereafter. Similarly, [28] applied intervals ranging from 50 °C to 70 °C for temperatures between 80 °C and 200 °C, and a much broader interval of 200 °C for the range between 400 °C and 1000 °C. These approaches make it difficult to capture subtle variations in bulk density associated with smaller temperature changes.

Despite the practical importance of mild temperature exposure in rock engineering, there is still limited understanding of how such conditions influence the bulk density of rocks. Most existing studies have focused on the effects of higher temperatures, leaving a knowledge gap in predicting rock behaviour under subsurface environments characterized by low to moderate thermal conditions. This study seeks to address this gap by examining variations in the bulk density of fine-grained granite (FGG) samples within the mild temperature range (20 °C–200 °C), using 20 °C increments. The specific objectives are: (1) to measure changes in mass, volume, and bulk density of FGG samples before, during, and after mild temperature treatments; (2) to identify the mechanisms driving these changes through scanning electron microscopy (SEM); and (3) to evaluate the engineering implications of these changes for subsurface applications. The research questions guiding this study are: (1) How does mild temperature affect the mass, volume, and bulk density of FGG? (2) What microscopic changes explain these variations in properties? (3) How can these findings be applied to improve geotechnical design in mild-temperature environments?

The novelty of this study lies in its focus on a narrow yet practically relevant temperature range (20 °C to 200 °C), examined at finer intervals of 20 °C. This approach enables a more detailed analysis of subtle changes in mass, volume, and density that are often overlooked in studies employing broader intervals or higher temperature ranges. By offering comprehensive insights into how fine-grained granite (FGG) responds both physically and microstructurally to mild thermal exposure, this study enhances predictive understanding of rock performance in subsurface environments characterized by low to moderate thermal conditions.

## 2. Materials and methods

Granite rock was collected from an outcrop in Ado-Ekiti, located in southwestern Nigeria. This granitic rock has a fine-grained texture and forms part of Nigeria's Precambrian basement complex [30, 31]. The mineralogical and physical properties of the samples were evaluated using recognized standard testing methods. Petrographic analysis was conducted to investigate mineralogical features, involving the preparation of thin sections examined under a polarizing microscope. Detailed image analysis and point counting were performed to determine the modal mineral composition, following the specifications of the International Society for Rock Mechanics (ISRM) [32].

For the assessment of physical properties—including water absorption, moisture content, porosity, density, and surface hardness—a series of tests were carried out in accordance with ISRM guidelines [33]. Porosity and dry density were determined using the saturation method. Samples were fully immersed in water for at least 24 hours to ensure saturation. Excess surface water was then removed with a damp cloth, and the saturated surface-dry mass was recorded. The samples were oven-dried at 105 °C for 24 hours, after which the dry mass was measured. The difference between saturated and dry masses was used to calculate pore volume, which was then expressed as a proportion of bulk volume to determine porosity. Dry unit weight was obtained by dividing the dry mass by the specimen's volume.

Schmidt hammer tests were performed using an N-type Schmidt

hammer with an impact energy of 2.207 Nm, in accordance with ISRM specifications [34]. Block samples were securely clamped to a rigid base to ensure stability during testing. The hammer was positioned perpendicular to the sample surface, and measurements were taken by a single operator. The resulting Schmidt Hammer Rebound (SHR) values were sorted in descending order, with the ten lowest values excluded; the average of the ten highest values was then calculated.

Point load strength was evaluated following Franklin's recommendations [35], with a minimum of three tests conducted to obtain a reliable average. Uniaxial compressive strength (UCS) tests were also performed on cylindrical specimens with approximate dimensions of 100 mm in length and 50 mm in diameter.

Cylindrical rock specimens, measuring 50 mm in diameter and 100 mm in height, were obtained from the same block without macro-cracks, in accordance with the recommendations of the [33] standard. Granite cores were extracted using a water-cooled diamond core drill to minimize heat generation and preserve sample integrity. The ends of the cores were carefully trimmed with a water-lubricated diamond saw blade to produce smooth, parallel surfaces. The specimens were then air-dried at room temperature in a well-ventilated laboratory for two weeks.

The mass and dimensions (diameter and length) of the air-dried specimens were measured using an electronic balance and a vernier caliper. Samples exhibiting atypical density were excluded, and the remaining specimens were grouped into sets of three. One group was not subjected to heat treatment and served as a control for comparison. The other specimens were heated to target temperatures of 40 °C, 60 °C, 80 °C, 100 °C, 120 °C, 140 °C, 160 °C, 180 °C, and 200 °C using an electric oven. The heating rate was maintained at 5 °C/min, and once the desired temperature was reached, it was held constant for two hours to ensure uniform heating throughout the specimens.

After two hours of exposure, the mass and dimensions (height and diameter) of the specimens were recorded under elevated conditions. The specimens were then returned to the oven and allowed to cool to room temperature, after which their mass and size were re-measured. The volume of each specimen was calculated using its height and diameter.

## 3. Results and discussion

### 3.1. Petrographic and physical properties of the rock

Figure 1 illustrates the principal petrographic features of the fine-grained granite (FGG). The mineral distribution and composition were determined using the point-counting method, while crystal sizes were measured macroscopically from photographs. Photomicrographs reveal that the FGG is primarily composed of biotite, quartz, and feldspar (both K-feldspar and plagioclase), with a minor presence of hornblende. The granite is homogeneous and densely packed, exhibiting crystal sizes ranging from 3 to 4 mm.

Biotite grains show a random arrangement, low relief, and irregular orientation, appearing dark to brown and occupying the interstices between surrounding minerals (Fig. 1). Some biotite crystals display acicular morphology. Microcline occurs as large, prominent grains with distinct grid twinning. Quartz appears as fine, transparent, angular crystals with sharp contacts. Hornblende is sparse, scattered, and varies in color from dark to straw-green (Fig. 1).

Table 1 presents the properties of fine-grained granite (FGG) obtained in accordance with relevant ISRM standards. The average porosity of the samples is 0.44%, which, according to the classification of the International Association for Engineering Geology and the Environment [36], falls within the “very low” category. This low porosity results from the compact interlocking of mineral grains, minimal microfractures, and uniform grain size distribution, all of which contribute to the rock's high strength and durability [37, 38].

The water content of the samples ranges from 0.045% to 0.092%, with an average of 0.06%, also classified as low by the International Association for Engineering Geology and the Environment [36]. This low water content is attributed to the fine-grained texture and strong

mineral bonding within the rock, which restricts moisture retention and enhances resistance to weathering [39].

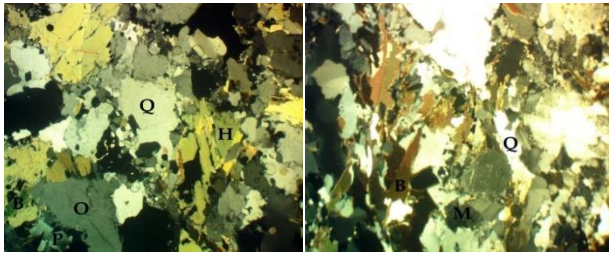


**Figure 1.** Photomicrograph of FGG under transmitted light. B: Biotite, M: Microcline; O: Orthoclase Feldspar; P: Plagioclase Feldspar; Q: Quartz. Bars 2 mm crossed polars.

**Table 1.** Physico-mechanical properties of the FGG.

Property	FGG
Water Content (%)	0.06
Porosity (%)	0.44
Density (g/cm <sup>3</sup> )	2.59
Water Absorption (%)	0.49
Point Load Strength (MPa)	17.12
Schmidt Rebound Hammer	57.8

The values reported in the table represent the mean of measurements taken from five rock specimens. The average of the top ten values was determined after excluding the ten lowest values to arrive at the Schmidt Rebound Hammer value.

In addition, the mean water absorption capacity of the FGG is 0.49%, indicating low permeability due to the freshness of feldspathic and ferromagnesian minerals and minimal weathering. This property supports the inference of low porosity and high structural integrity. According to [40], rocks with such characteristics are typically resistant to moisture-induced degradation, thereby enhancing their long-term durability in engineering applications.

The average density of the rock samples is 2.59 g/cm<sup>3</sup>, classified as high by the International Association for Engineering Geology and the Environment [36], and is consistent with the rock's low porosity and tightly interlocked mineral constituents. The average point load strength index of 17.17 MPa categorizes the rock as very strong. This high strength can be attributed to its mineralogical composition, particularly the presence of quartz, which is well known for its resistance to deformation. The Schmidt Rebound Hammer mean value of 57.8 further confirms the rock's high hardness and surface strength, making it suitable for structural and geotechnical engineering applications where mechanical durability is essential.

### 3.2. Influence of mild temperature treatment on mass of the granitic rock samples

Table 2 shows the mass of FGG specimens prior to, during, and after different predetermined temperatures. The percentage change in mass ( $\tau_m$ ) of each fine-grained granite specimen was defined as follows:

$$\tau_{mu} = \frac{m_o - m_u}{m_o} * 100 \quad (1)$$

$$\tau_{ma} = \frac{m_o - m_a}{m_o} * 100 \quad (2)$$

Where  $\tau_{mu}$  and  $\tau_{ma}$  are, respectively, the mass change of rock specimens during and after thermal treatment.  $m_o$ ,  $m_u$ , and  $m_a$  are, respectively, the masses of the granitic rock specimens before, under and after the mild temperature treatments. Fig. 2 shows the plot of  $\tau_{mu}$  and  $\tau_{ma}$  against temperature for the fine-grained granite specimens. The average percentage mass loss of the granitic rock exhibits an upward trend with increasing temperature. The percentage mass loss increased sharply after the temperature rose beyond 80° C (Fig. 2). When the temperature was less than 100 °C (both during and after temperature

treatments), the average mass loss of the granitic rock was low, and the percentage mass loss is less than 0.04%.

The decrease in mass of the rock specimens may be attributed to the generation of rock fragments and the evaporation or partial loss of structural water. Different forms of water present in rocks are released at varying temperature ranges [41]. Specifically, "evaporation of absorbed water" occurs between 50 °C and 100 °C, "release of bonded water" between 150 °C and 300 °C, "release of crystal water" between 250 °C and 400 °C, and "release of structural water" between 300 °C and 500 °C [19]. Since fine-grained granite (FGG) is composed mainly of quartz, biotite, and feldspar—minerals that rarely undergo thermochemical reactions releasing water within this temperature range—the observed percentage mass decrease remains below 0.15%.

Similarly, the average percentage mass loss of granitic rock during exposure to the mild temperature range is higher than that recorded after cooling. [12] reported comparable behaviour while investigating the effects of elevated temperatures—up to 1000 °C—on the bulk density of granitic rock. This difference may be attributed to environmental moisture infiltrating the specimens during the oven cooling process. Furthermore, [42] observed that the percentage mass loss of granite specimens subjected to rapid quenching is lower than that of specimens cooled more gradually.

When compared with previous studies on granites and other rock types, clear differences emerge in the relationship between temperature and the extent of mass reduction across various rocks after thermal treatment. Granites typically exhibit mass decrease rates of less than 0.4%, even when heated to 1000 °C, since their constituent minerals rarely undergo thermochemical reactions that release water or gas upon heating. At temperatures below 200 °C, the mass reduction rate in granite is generally less than 0.06% [42, 43], primarily due to the "evaporation of absorbed water" and the "release of bound water" [19].

For carbonate rocks, mass decrease below 200 °C is generally less than 0.1% or negligible, attributed to the evaporation of bound and constitution water. However, above 400 °C, a significant increase occurs due to the breakdown of carbonate minerals [44, 45]. Sandstone and claystone containing clay minerals show a more pronounced reduction in mass with increasing temperature, largely due to the decomposition and desorption of clay minerals [12, 46]. For instance, claystone exhibits approximately 2% mass loss after treatment at 200 °C [28], while sandstone shows about 0.5% mass loss at the same temperature [46]. In contrast, [10] reported no measurable mass loss in either coarse- or fine-grained sandstone after treatment at 200 °C.

### 3.3. Influence of mild temperature treatment on volume of the granitic rock samples

Table 2 presents the volume of the fine-grained granite specimens before, during, and after the different predetermined temperatures. We defined the volume change ( $\tau_v$ ) of the fine-grained granite specimens as follows:

$$\tau_{vu} = \frac{V_u - V_o}{V_o} * 100 \quad (3)$$

$$\tau_{va} = \frac{V_a - V_o}{V_o} * 100 \quad (4)$$

Where  $\tau_{vu}$  and  $\tau_{va}$  are, respectively, the variation in the volume of the rock specimens during, and after temperature treatment.  $V_o$ ,  $V_u$ , and  $V_a$  are, respectively, the volumes of the granitic rock specimens before, during, and after the mild temperature treatments. Figure 3 shows the plot of the average  $\tau_{vu}$  and  $\tau_{va}$  against temperature for the fine-grained granite specimens.

Fig. 3 shows that the average  $\tau_{vu}$  and  $\tau_{va}$  increased with a rise in temperature. The rise in average  $\tau_{vu}$  and  $\tau_{va}$  is, however, not more than 0.6% and 0.4%, respectively.

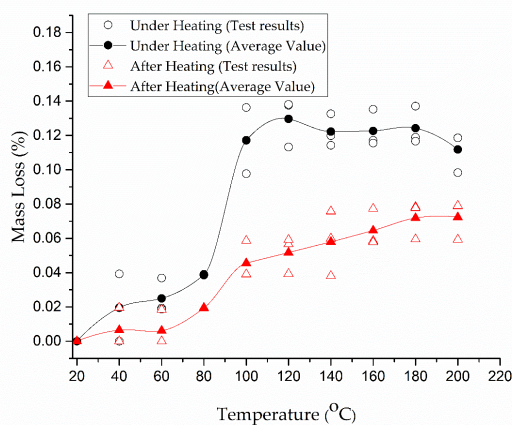
The volume increase in the rock specimens following exposure to the mild temperature treatments may be attributed to the thermal expansion and reactions of the rock constituent minerals, as well as irrecoverable structural deformation caused by the formation of microcracks [8, 12].



**Table 2.** The density, mass, and volume of granite specimens during and after the mild temperature treatment.

Temp (°C)	Mass		Volume			Density			
	m <sub>o</sub> (g)	m <sub>u</sub> (g)	m <sub>a</sub> (g)	V <sub>o</sub> (cm <sup>3</sup> )	V <sub>u</sub> (cm <sup>3</sup> )	V <sub>a</sub> (cm <sup>3</sup> )	ρ <sub>o</sub> (g/cm <sup>3</sup> )	ρ <sub>u</sub> (g/cm <sup>3</sup> )	ρ <sub>a</sub> (g/cm <sup>3</sup> )
20	514	-	-	180.98	-	-	2.84	-	-
	505.3	-	-	184.83	-	-	2.73	-	-
	512.6	-	-	184.83	-	-	2.77	-	-
40	509.7	509.5	509.6	180.98	180.98	180.98	2.82	2.82	2.82
	526.3	526.3	526.3	188.6	188.6	188.6	2.79	2.79	2.79
	513	512.9	513	188.6	188.6	188.6	2.72	2.72	2.72
60	516.4	516.3	516.4	188.6	189.21	189	2.74	2.73	2.73
	534.6	534.5	534.6	198.34	198.81	198.74	2.70	2.69	2.69
	542.4	542.2	542.3	196.38	197.06	196.38	2.76	2.75	2.76
80	511.6	511.4	511.5	195.39	196.0	195.59	2.62	2.61	2.62
	519.1	518.9	519	196.38	197.1	196.77	2.64	2.63	2.64
	518	517.8	517.9	195.59	196.28	196.18	2.65	2.64	2.64
100	511.8	511.2	511.5	194.81	195.5	195.31	2.63	2.61	2.62
	513.6	512.9	513.4	192.47	193.31	193.1	2.67	2.65	2.66
	512.0	511.5	511.8	192.47	193.19	192.88	2.66	2.65	2.65
120	529.8	529.2	529.5	196.38	197.23	197.1	2.70	2.68	2.69
	508.8	508.1	508.6	192.86	193.72	193.4	2.64	2.62	2.63
	507	506.3	506.7	187.09	187.98	187.67	2.71	2.69	2.70
140	527.9	527.2	527.5	197.36	198.35	198.14	2.67	2.66	2.66
	525.2	524.6	525	195.59	196.51	196.33	2.69	2.67	2.67
	500.5	499.9	500.2	194.41	195.38	195.15	2.57	2.56	2.56
160	512.2	511.6	511.9	194.81	195.84	195.61	2.63	2.61	2.62
	519.3	518.7	519	196.38	197.4	197.2	2.64	2.63	2.63
	517.6	516.9	517.2	188.6	189.5	189.3	2.74	2.73	2.73
180	504.6	504	504.3	195.59	196.63	196.41	2.58	2.56	2.57
	510.7	510	510.3	190.54	191.44	191.3	2.68	2.66	2.67
	514.5	513.9	514.1	192.47	193.55	193.31	2.67	2.66	2.66
200	508.6	508.1	508.2	186.71	187.8	187.54	2.72	2.71	2.71
	505.9	505.3	505.6	190.54	191.5	191.45	2.66	2.64	2.64
	506.1	505.5	505.7	191.5	192.57	192.17	2.64	2.62	2.63

m<sub>o</sub> mass before heating, m<sub>u</sub> mass under heating, m<sub>a</sub> mass after heating, v<sub>o</sub> volume before heating, v<sub>u</sub> volume under heating, v<sub>a</sub> volume after heating, ρ<sub>o</sub> volume before heating, ρ<sub>u</sub> volume under heating, ρ<sub>a</sub> volume after heating, FGG fine-grained granite.

**Figure 2.** Mass change rate in tested granitic rock specimens against temperature.

According to [47], variations in the thermal expansion properties of different mineral constituents within a rock may lead to structural damage along mineral boundaries. Similarly, differences in thermal behaviour and expansion across various crystallographic axes of the

same mineral can induce thermal stresses [48]. When the thermal stress exceeds the tensile or shear strength of the rock, new micro-cracks are initiated [27]. At 100 °C, quartz exhibits a thermal expansion of 0.14 normal to the C-axis and 0.08 along the C-axis, as reported by [49]. Plagioclase feldspar shows thermal expansion values of 0.09 along the A-axis and 0.03 normal to the O10-axis.

Similarly, the average volume increase of fine-grained granite (FGG) during mild temperature treatment is greater than that observed after cooling (Fig. 3). [12] reported similar behaviour while examining the effects of elevated temperatures up to 1000 °C on the bulk density of granitic rock. Within the mild temperature range, the increase in rock volume can be attributed to the dilation of constituent minerals and the initiation of micro-cracks. After thermal treatment and subsequent cooling, the expanded minerals contract; however, the structural damage caused by newly formed micro-cracks is irreversible. Consequently, the average size of the rock during heating is higher than the average volume increase measured after exposure.

At temperatures below 200 °C, certain rocks such as sandstone [29], claystone [28], marble [6], limestone [50], and granite [43, 51] exhibit a negative rate of volume change, indicating contraction. In contrast, rocks such as sandstone [46] and granite [12, 52] show positive but small volume increases—less than 1%—suggesting slight expansion below 200 °C. According to [53], this contraction may result from the evolution of initial micropores and microcracks within the rocks, which create space for mineral expansion at temperatures below 200 °C.

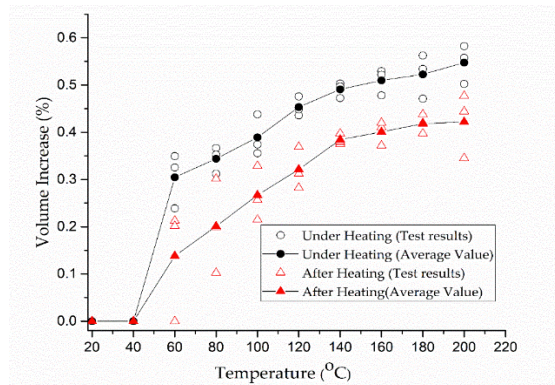


**Figure 3.** Rate of volume change in tested granitic rock specimens with temperature.

### 3.4. Influence of the mild temperature on the bulk density of the granitic rock samples

The density of the fine-grained specimens before, under, and after different predetermined temperatures is presented in Table 2. The percentage change in density ( $\tau_p$ ) of the FGG specimens is as follows:

$$\tau_{pu} = \frac{\rho_o - \rho_u}{\rho_o} * 100 \quad (5)$$

$$\tau_{pa} = \frac{\rho_o - \rho_a}{\rho_o} * 100 \quad (6)$$

Where  $\tau_{pu}$  and  $\tau_{pa}$  are, respectively, the change in the density of the rock specimens under and after temperature treatment.  $\rho_o$ ,  $\rho_u$  and  $\rho_a$  are the densities of the granitic rock specimens before, under, and after the mild temperature treatment. Fig. 4 displays the plot of the average  $\tau_{pu}$  and  $\tau_{pa}$  against temperature for the rock specimens. The reduction in mass coupled with the expansion in volume of the rock samples are responsible for the variation observed in the density of the rock during and after temperature treatment. Although the average percentage change in mass is lower compared to the percentage change in volume, the relationship between the average  $\tau_{pu}$  and  $\tau_{pa}$  and temperature is like that of the percentage increase in volume and temperature (Fig. 4). The average values of  $\tau_{pu}$  and  $\tau_{pa}$  increased slowly with a rise in temperature. The final increase in average  $\tau_{pu}$  and  $\tau_{pa}$  is, however, not more than 0.65% and 0.5%, respectively. Similarly, the average values of  $\tau_p$  during mild temperature treatment are higher than those after exposure to mild temperature treatment. Compared to earlier investigations on granites and other rock types, the density variations in rocks are minimal, typically less than 1%, at temperatures below 200°C [6, 12, 28]. However, above this temperature range, the rock densities experience a rapid increase.

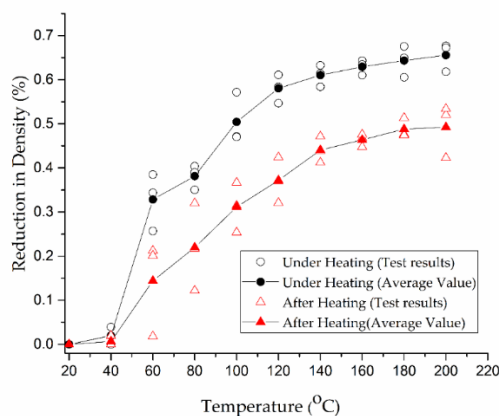


**Figure 4.** Rate of change in density of fine-grained granite against temperature.

### 3.5. Microscopic observation

According to [54], microcracks in rocks can be classified as intra-granular (within a single grain), inter-granular (along grain boundaries), or trans-granular (cutting across multiple grains). Figure 5 presents SEM images showing the effects of various predetermined mild temperatures on the granitic rock samples. At room temperature, few or no microcracks are visible, and most mineral grains in the fine-grained granite (FGG) appear closely packed. The limited microcracks observed at ambient conditions are intra-granular, occurring more frequently in feldspar and quartz than in biotite (Fig. 5a).

In specimens exposed to temperatures between 40 °C and 80 °C, intra-granular microcracks were also identified (Fig. 5b–d), particularly in quartz, plagioclase feldspar, and K-feldspar, while biotite grains occasionally exhibited such cracks. At 60–80 °C (Fig. 5c–d), inter-granular microcracks appeared along boundaries between biotite and quartz, or between quartz and feldspar grains.

More thermally induced microcracks were observed in samples heated to 100–140 °C (Fig. 5e–g), occurring both within mineral grains and along inter-crystalline boundaries. Inter-granular cracks were found between feldspar grains (K-feldspar boundaries), between feldspar and quartz (quartz–plagioclase/K-feldspar boundaries), and between biotite and feldspar (K-feldspar–biotite boundaries). Intra-granular cracks became larger at this temperature range and were also noted in biotite grains. Above 140 °C, intra-granular cracks became common in biotite.

At 160–180 °C (Fig. 5h–i), both intra- and inter-granular microcracks were evident. At 200 °C (Fig. 5j), thermally induced microcracks of all three types—intra-granular, inter-granular, and trans-granular—were observed within, between, and across mineral grains. Trans-granular cracks, though few, were found across feldspar grains (plagioclase and K-feldspar). The size of inter-granular cracks increased with rising temperature, and some intra-granular cracks propagated and coalesced with inter-granular cracks above 80 °C.

One of the primary reasons for microcrack development in rocks containing different minerals, according to [55], is the discrepancy in thermal expansion coefficients among these minerals. Compared with quartz and feldspar, biotite has lower heat capacity and thermal conductivity, which explains why intra-granular microcracks appeared earlier in quartz and feldspar than in biotite.

## 4. Conclusions

This study investigated the effects of mild thermal exposure (20 °C–200 °C) on the bulk density of fine-grained granite (FGG), aiming to address the limited understanding of rock behaviour under low-temperature conditions relevant to rock engineering applications such as geothermal systems, radioactive waste repositories, and post-fire infrastructure rehabilitation. The specific objectives were: (1) to measure changes in mass, volume, and bulk density of FGG before, during, and after mild thermal treatments; (2) to identify the mechanisms driving these changes using scanning electron microscopy (SEM); and (3) to assess the engineering implications for subsurface and thermally influenced environments.

The results confirm that bulk density decreases due to mass loss and volume increase during and after mild thermal treatments. Although both mass loss and volume expansion increase with temperature, the percentage increase in volume consistently exceeds that of mass loss, leading to a net reduction in bulk density. These effects were more pronounced during heating than after cooling. Notably, the maximum average mass loss (0.04%), volume increase (0.2%), and density reduction (0.25%) observed at temperatures above 100 °C remain relatively small compared with changes reported under high-temperature regimes (>300 °C). Mass loss is primarily attributed to moisture evaporation and mineral dehydration, while volume expansion results from thermal expansion and the formation of microcracks. SEM analysis confirmed a progressive increase in microcrack density with temperature, with transgranular cracking

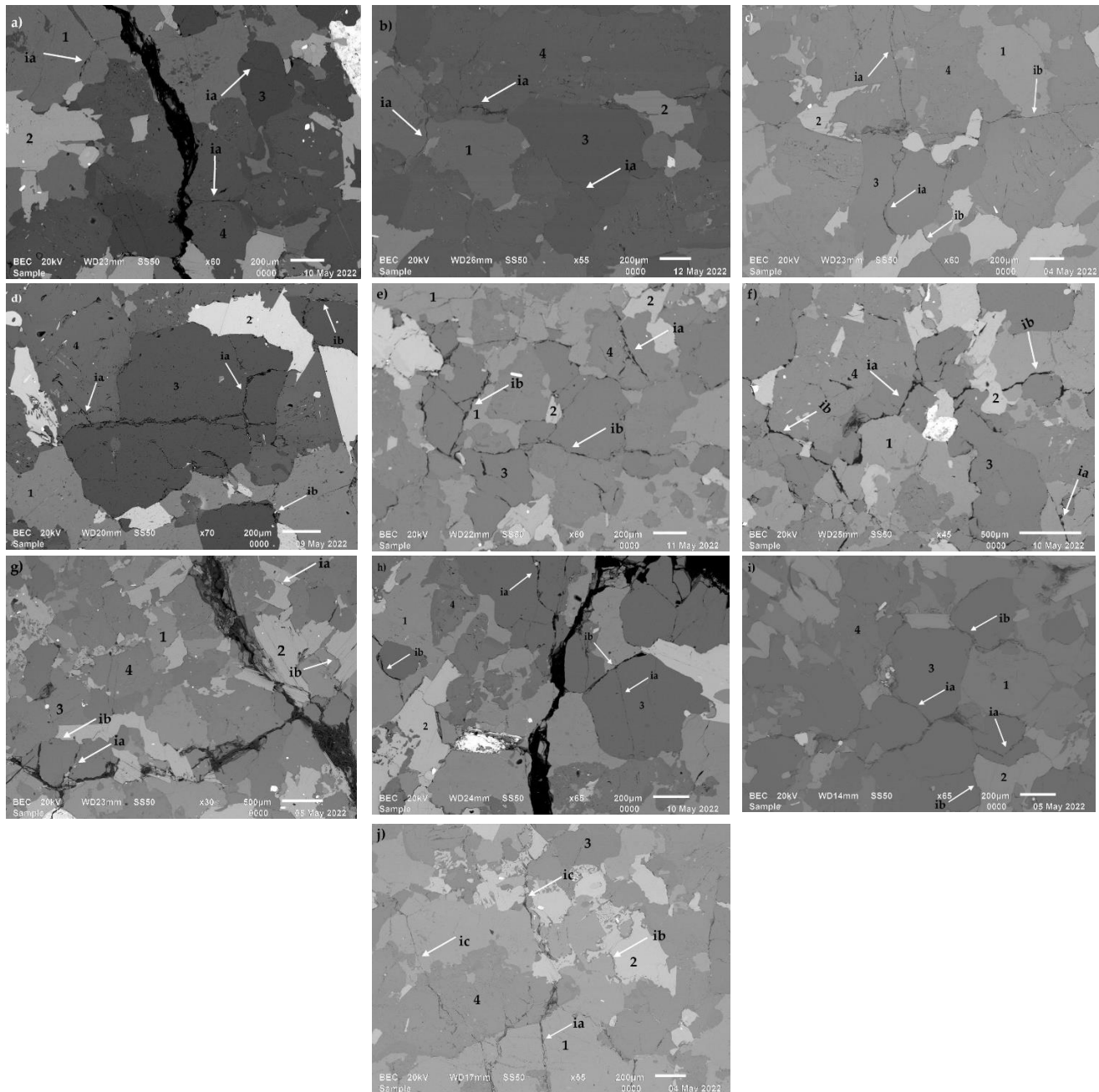


**Figure 5.** Microscopic examinations of the granite specimens following mild-temperature treatments. a) 20°C b) 40°C c) 60°C d) 80°C e) 100°C f) 120°C g) 140°C h) 160°C i) 180°C j) 200°C 1: K-feldspar; 2: Biotite; 3: Quartz; 4: Plagioclase; ia: intra-granular microcracks; ib: inter-granular microcracks; ic: trans-granular microcracks

observed across feldspar grains at 200 °C.

From an engineering perspective, these findings provide valuable input for the design and assessment of geotechnical systems in mild thermal environments. The relatively modest decrease in bulk density suggests that fine-grained granite retains its structural integrity under low-temperature exposure, which is advantageous for long-term performance in applications such as radioactive waste isolation, geothermal reservoir development, and fire-affected tunnel maintenance. However, while the changes are small, they are not negligible and may accumulate or interact with other stressors over time. Therefore, the study underscores the importance of considering even mild thermal effects in design calculations, particularly for long-term or safety-critical subsurface projects. Future research should extend this work by examining complementary mechanical properties (e.g., strength, permeability) under similar thermal conditions to

provide a more comprehensive understanding of granite performance in these settings.

### Acknowledgement

We thank laboratory staff in the Department of Geology, University of The Free State, where SEM was carried out, and Ms. Megan Welman-Purchase for her help during the analysis.

### References

- [1]. Kumari, W. G. P., Ranjith, P. G., Perera, M. S. A., Shao, S., Chen, B. K., Lashin, A., Rathnaweera, T. D. (2017). Mechanical behaviour of Australian Strathbogie granite under in-situ stress



- and temperature conditions: An application to geothermal energy extraction. *Geothermics*, 65, 44–59. <https://doi.org/10.1016/j.geothermics.2016.07.002>
- [2]. Xiao, Y., Yin, J., Hu, Y., Wang, J., Yin, H., & Qi, H. (2019). Monitoring and Control in Underground Coal Gasification: Current Research Status and Future Perspective. *Sustainability* 2019, Vol. 11, Page 217, 11(1), 217. <https://doi.org/10.3390/SU11010217>
- [3]. Sun, F., Yao, Y., Chen, M., Li, X., Zhao, L., Meng, Y., ... Feng, D. (2017). Performance analysis of superheated steam injection for heavy oil recovery and modeling of wellbore heat efficiency. *Energy*, 125, 795–804. <https://doi.org/10.1016/j.energy.2017.02.114>
- [4]. Ranjith, P. G., Viete, D. R., Chen, B. J., & Perera, M. S. A. (2012). Transformation plasticity and the effect of temperature on the mechanical behaviour of Hawkesbury sandstone at atmospheric pressure. *Engineering Geology*, 151, 120–127.
- [5]. Lintao, Y., Marshall, A. M., Wanatowski, D., Stace, R., & Ekneligoda, T. (2017). Effect of high temperatures on sandstone – a computed tomography scan study. *https://doi.org/10.1680/jphmg.15.00031*, 17(2), 75–90. <https://doi.org/10.1680/JPHMG.15.00031>
- [6]. Ozguven, A., & Ozelcelik, Y. (2014). Effects of high temperature on physico-mechanical properties of Turkish natural building stones. *Engineering Geology*, 183, 127–136. <https://doi.org/10.1016/j.enggeo.2014.10.006>
- [7]. Zhang, W., Sun, Q., Zhang, Y., Xue, L., & Kong, F. (2018). Porosity and wave velocity evolution of granite after high-temperature treatment: a review. *Environmental Earth Sciences*, 77(9), 350. <https://doi.org/10.1007/s12665-018-7514-3>
- [8]. Zhu, Z., Tian, H., Chen, J., Jiang, G., Dou, B., Xiao, P., & Mei, G. (2020). Experimental investigation of thermal cycling effect on physical and mechanical properties of heated granite after water cooling. *Bulletin of Engineering Geology and the Environment*, 79(5), 2457–2465. <https://doi.org/10.1007/s10064-019-01705-w>
- [9]. Chen, S., Yang, C., & Wang, G. (2017). Evolution of thermal damage and permeability of Beishan granite. *Applied Thermal Engineering*, 110, 1533–1542. <https://doi.org/10.1016/j.applthermaleng.2016.09.075>
- [10]. Lintao, Y., Marshall, A. M., Wanatowski, D., Stace, R., & Ekneligoda, T. (2017). Effect of high temperatures on sandstone - a computed tomography scan study. *International Journal of Physical Modelling in Geotechnics*, 17(2), 75–90. <https://doi.org/10.1680/jphmg.15.00031>
- [11]. Zhao, Z., Liu, Z., Pu, H., & Li, X. (2018). Effect of Thermal Treatment on Brazilian Tensile Strength of Granites with Different Grain Size Distributions. *Rock Mechanics and Rock Engineering*, 51(4), 1293–1303. <https://doi.org/10.1007/s00603-018-1404-6>
- [12]. Zhu, Z., Tian, H., Jiang, G., & Dou, B. (2022). Effects of high temperature on rock bulk density. *Geomechanics and Geoengineering*, 17(2), 647–657. <https://doi.org/10.1080/17486025.2020.1827169>
- [13]. Ferrero, A. M., & Marini, P. (2001). Technical note: Experimental studies on the mechanical behaviour of two thermal cracked marbles. *Rock Mechanics and Rock Engineering*, 34(1), 57–66. <https://doi.org/10.1007/s006030170026>
- [14]. Glover, P. W. J., Baud, P., Darot, M., Meredith, P. G., Boon, S. A., LeRavalec, M., ... Reuschlé, T. (1995).  $\alpha/\beta$  phase transition in quartz monitored using acoustic emissions. *Geophysical Journal International*, 120(3), 775–782. <https://doi.org/10.1111/j.1365-246X.1995.tb01852.x>
- [15]. Griffiths, L., Heap, M. J., Baud, P., & Schmittbuhl, J. (2017). Quantification of microcrack characteristics and implications for stiffness and strength of granite. *International Journal of Rock Mechanics and Mining Sciences*, 100, 138–150. <https://doi.org/10.1016/j.ijrmms.2017.10.013>
- [16]. Mahanta, B., Singh, T. N., & Ranjith, P. G. (2016). Influence of thermal treatment on mode I fracture toughness of certain Indian rocks. *Engineering Geology*, 210, 103–114. <https://doi.org/10.1016/j.enggeo.2016.06.008>
- [17]. Yin, T., Li, X., Cao, W., & Xia, K. (2015). Effects of Thermal Treatment on Tensile Strength of Laurentian Granite Using Brazilian Test. *Rock Mechanics and Rock Engineering*, 48(6), 2213–2223. <https://doi.org/10.1007/s00603-015-0712-3>
- [18]. Tian, H., Kempka, T., Xu, N. X., & Ziegler, M. (2012). Physical properties of sandstones after high temperature treatment. *Rock Mechanics and Rock Engineering*, 45(6), 1113–1117. <https://doi.org/10.1007/s00603-012-0228-z>
- [19]. Wong, L. N. Y., Zhang, Y., & Wu, Z. (2020). Rock strengthening or weakening upon heating in the mild temperature range? *Engineering Geology*, 272, 105619. <https://doi.org/10.1016/j.enggeo.2020.105619>
- [20]. Zhang, L., Mao, X., & Lu, A. (2009). Experimental study on the mechanical properties of rocks at high temperature. *Science in China, Series E: Technological Sciences*, 52(3), 641–646. <https://doi.org/10.1007/s11431-009-0063-y>
- [21]. Wong, L. N. Y., & Zhang, Y. H. (2019, June 23). Numerical Investigation of Micromechanisms of Thermal Strengthening in Rock. *OnePetro*. Retrieved from /ARMAUSRMS/proceedings-abstract/ARMA19/All-ARMA19/124676
- [22]. Wadhams, N. (2011). Gold Standards: How miners dig for riches in a 2-mile-deep furnace. *Wired*, 19(3), 42.
- [23]. Olasolo, P., Juárez, M. C., Morales, M. P., Damico, S., & Liarte, I. A. (2016). Enhanced geothermal systems (EGS): A review. *Renewable and Sustainable Energy Reviews*, 56, 133–144. <https://doi.org/10.1016/j.rser.2015.11.031>
- [24]. Hökmark, H., & Fälth, B. (2003). Thermal dimensioning of the deep repository-Influence of canister spacing, canister power, rock thermal properties and nearfield design on the maximum canister surface temperature.
- [25]. Soppe, W. J., Donker, H., Celma, A. G., & Prij, J. (1994). Radiation-induced stored energy in rock salt. *Journal of Nuclear Material*, 217(1–2), 1–31. [https://doi.org/https://doi.org/10.1016/0022-3115\(94\)90301-8](https://doi.org/https://doi.org/10.1016/0022-3115(94)90301-8)
- [26]. Yavuz, H., Demirdag, S., & Caran, S. (2010). Thermal effect on the physical properties of carbonate rocks. *International Journal of Rock Mechanics and Mining Sciences*, 47(1), 94–103. <https://doi.org/10.1016/j.ijrmms.2009.09.014>
- [27]. Yang, S.-Q., Ranjith, P. G., Jing, H.-W., Tian, W.-L., & Ju, Y. (2017). An experimental investigation on thermal damage and failure mechanical behavior of granite after exposure to different high temperature treatments. *Geothermics*, 65, 180–197. <https://doi.org/10.1016/j.geothermics.2016.09.008>
- [28]. Tian, H., Ziegler, M., & Kempka, T. (2014). Physical and mechanical behavior of claystone exposed to temperatures up to 1000 °C. *International Journal of Rock Mechanics and Mining Sciences*, 70, 144–153. <https://doi.org/10.1016/j.ijrmms.2014.04.014>
- [29]. Wu, G., Wang, Y., Swift, G., & Chen, J. (2013). Laboratory Investigation of the Effects of Temperature on the Mechanical Properties of Sandstone. *Geotechnical and Geological Engineering* 2013 31:2, 31(2), 809–816. <https://doi.org/10.1007/S10706-013-9614-X>
- [30]. Afolagboye, L. O. (2021). Using index tests to predict the

- compressive strength of crystalline rocks. *Proceedings of the Institution of Civil Engineers - Construction Materials*, 174(6), 289–297. <https://doi.org/10.1680/jcoma.18.00061>
- [31]. Talabi, A. O., & Tijani, M. N. (2013). Hydrochemical and stable isotopic characterization of shallow groundwater system in the crystalline basement terrain of Ekiti area, southwestern Nigeria. *Applied Water Science*, 3(1), 229–245. <https://doi.org/10.1007/s13201-013-0076-3>
- [32]. ISRM, (International Society for Rock Mechanics). (1978). Suggested method for petrographic description of rocks. Commission for standardization of laboratory and field tests. *International Journal of Rock Mechanics and Mining Sciences & Geomechanics Abstracts*, 15(2), 43–45.
- [33]. ISRM, (International Society for Rock Mechanics). (2007). The complete ISRM suggested methods for rock characterization, testing and monitoring: 1974–2006. In R. Ulusay & J. A. Hudson (Eds.), *Suggested methods prepared by the commission on testing methods* (p. 628). Ankara, Turkey: Kozan Offset.
- [34]. ISRM. (1981). ISRM suggested methods: rock characterization. In E. T. Brown (Ed.), *Testing and monitoring*. London: Pergamon.
- [35]. Franklin, J. A. (1985). Suggested method for determining point load strength. *International Journal of Rock Mechanics and Mining Sciences & Geomechanics Abstracts*, 22(2), 51–60. [https://doi.org/10.1016/0148-9062\(85\)92327-7](https://doi.org/10.1016/0148-9062(85)92327-7)
- [36]. IAEG. (1979). Classification of rocks and soils for engineering geological mapping part I: Rock and soil materials. *Bulletin of the International Association of Engineering Geology*, 19(1), 364–371. <https://doi.org/10.1007/BF02600503>
- [37]. Afolagboye, L. O., Talabi, A. O., & Owoyemi, O. O. (2024). Slake Durability of Granitic Rocks in Wet and Dry Conditions. In M. Bezzeghoud, Z. A. Ergüler, J. Rodrigo-Comino, M. K. Jat, R. Kalatehjari, D. S. Bisht, ... M. Gentilucci (Eds.), *Recent Research on Geotechnical Engineering, Remote Sensing, Geophysics and Earthquake Seismology* (pp. 65–68). Cham: Springer Nature Switzerland.
- [38]. Afolagboye, L. O., Owoyemi, O. O., & Akinola, O. O. (2023). Effect of pH Condition and Different Solution on the Slake Durability of Granitic Rocks. *Geotechnical and Geological Engineering*, 41(2), 897–906. <https://doi.org/10.1007/S10706-022-02312-5/METRICS>
- [39]. Cai, X., Zhou, Z., Liu, K., Du, X., & Zang, H. (2019). Water-Weakening Effects on the Mechanical Behavior of Different Rock Types: Phenomena and Mechanisms. *Applied Sciences* 2019, Vol. 9, Page 4450, 9(20), 4450. <https://doi.org/10.3390/APP9204450>
- [40]. Bell, F. G. (2007). *Engineering geology* (2nd ed.). Elsevier: Oxford.
- [41]. Zhang, W., & Sun, Q. (2018). Identification of Primary Mineral Elements and Macroscopic Parameters in Thermal Damage Process of Limestone with Canonical Correlation Analysis. *Rock Mechanics and Rock Engineering*, 51(4), 1287–1292. <https://doi.org/10.1007/s00603-018-1401-9>
- [42]. Jin, P., Hu, Y., Shao, J., Zhao, G., Zhu, X., & Li, C. (2019). Influence of different thermal cycling treatments on the physical, mechanical and transport properties of granite. *Geothermics*, 78(December 2018), 118–128. <https://doi.org/10.1016/j.geothermics.2018.12.008>
- [43]. Zhang, W., Sun, Q., Hao, S., Geng, J., & Lv, C. (2016). Experimental study on the variation of physical and mechanical properties of rock after high temperature treatment. *Applied Thermal Engineering*, 98, 1297–1304. <https://doi.org/10.1016/J.APPLTHERMALENG.2016.01.010>
- [44]. Meng, Q. Bin, Wang, C. K., Liu, J. F., Zhang, M. W., Lu, M. M., & Wu, Y. (2020). Physical and micro-structural characteristics of limestone after high temperature exposure. *Bulletin of Engineering Geology and the Environment*, 79(3), 1259–1274. <https://doi.org/10.1007/s10064-019-01620-0>
- [45]. Zhang, W., Qian, H., Sun, Q., & Chen, Y. (2015). Experimental study of the effect of high temperature on primary wave velocity and microstructure of limestone. *Environmental Earth Sciences*, 74(7), 5739–5748. <https://doi.org/10.1007/S12665-015-4591-4/METRICS>
- [46]. Yang, S. Q., Xu, P., Li, Y. B., & Huang, Y. H. (2017). Experimental investigation on triaxial mechanical and permeability behavior of sandstone after exposure to different high temperature treatments. *Geothermics*, 69, 93–109. <https://doi.org/10.1016/J.GEOTHERMICS.2017.04.009>
- [47]. Gautam, P. K., Verma, A. K., Jha, M. K., Sharma, P., & Singh, T. N. (2018). Effect of high temperature on physical and mechanical properties of Jalore granite. *Journal of Applied Geophysics*, 159, 460–474. <https://doi.org/10.1016/j.jappgeo.2018.07.018>
- [48]. Somerton, W. H. (1992). *Thermal properties and temperature-related behavior of rock/fluid systems*. Amsterdam: Elsevier.
- [49]. Clark, S. P. (1966). *Handbook of Physical Constants*. The Geological Society of America, 97, 459–482. <https://doi.org/10.1130/MEM97>
- [50]. Wu, G., Teng, N. G., & Wang, Y. (2011). Physical and mechanical characteristics of limestone after high temperature. *Chinese Journal of Geotechnical Engineering*, 33, 259–264.
- [51]. Xu, X. L., Gao, F., & Zhang, Z. Z. (2014). Influence of confining pressure on deformation and strength properties of granite after high temperatures. *Chinese Journal of Geotechnical Engineering*, 36, 2246–2252.
- [52]. Hu, J., Sun, Q., & Pan, X. (2018). Variation of mechanical properties of granite after high-temperature treatment. *Arabian Journal of Geosciences*, 11(2), 1–8. <https://doi.org/10.1007/S12517-018-3395-8/METRICS>
- [53]. Zhu, Z. nan, Tian, H., Jiang, G. sheng, & Cheng, W. (2018). Effects of High Temperature on the Mechanical Properties of Chinese Marble. *Rock Mechanics and Rock Engineering*, 51(6), 1937–1942. <https://doi.org/10.1007/S00603-018-1426-0/METRICS>
- [54]. Freire-Lista, D. M., Fort, R., & Varas-Muriel, M. J. (2016). Thermal stress-induced microcracking in building granite. *Engineering Geology*, 206, 83–93. <https://doi.org/10.1016/J.ENGGEOL.2016.03.005>
- [55]. Gómez-Heras, M., Smith, B. J., & Fort, R. (2006). Surface temperature differences between minerals in crystalline rocks: Implications for granular disaggregation of granites through thermal fatigue. *Geomorphology*, 78(3–4), 236–249. <https://doi.org/10.1016/J.GEOMORPH.2005.12.013>